Article

Study on the Degradation of Nano-Scale MOF under Physiological Conditions by Detecting Ligands

Jinchao Liu [1], Songhai Wu [1,*]

[1] School of Chemical Engineering and Technology, Tianjin University, Tianjin 300350, China; 15830600407@163. com
* Correspondence: wusonghai@tju.edu.cn; Tel.: +86-138-2088-8127

Abstract: Metal organic frameworks (MOFs) composed of metal ions and multifunctional organic ligands are one of the most attractive porous materials. Their potential applications in gas storage, separation, catalysis, biomedicine and many other fields have attracted much attention. In this study, Nano-Mn-MOF-74 with nano size were successfully synthesized by adding acetic acid and characterized it by SEM, TEM and XRD. Furthermore, a new method to trace the degradation process of nanoMOFs through detection of ligand concentration under physiological conditions was developed.

Keywords: Metal organic framework; Mn-MOF-74; nanomaterial; degradation

1. Introduction

Metal organic frameworks (MOFs) are crystalline porous materials with periodic network structure formed by self-assembly of metal ions and organic ligands [1]. When assembled on a nanoscale, they are called nanoMOFs [2]. The chemical variability of the modules makes MOFs have corresponding characteristics. They can be adjusted and changed for different applications, including gas storage, catalysis, sensing and optics [3,4]. Particularly, nanoMOFs can be applied in biomedical field. In such applications, nanoMOFs are mainly used as passive delivery carriers for other bioactive agents [5-7]. People are more and more interested in exploring metal nodes or organic connectors of MOFs for cancer treatment or bacterial infection treatment [8-10]. However, little is known about the degradation of these nanomaterials under physiological conditions. Therefore, the degradation process should be investigated before the practical application of nanoMOFs.

Mn-MOF-74 is formed by Mn ion and 2,5-dihydroxyterephthalic acid (2OH-BDO), which has hexagonal pore structure and is widely used in catalysis and adsorption [11,12]. In previous studies, manganese oxide nanoparticles have been confirmed to be useful for cancer immunotherapy [13-15]. In particular, recent studies have reported that Mn ion is an effective innate immune stimulant *in vitro* and *in vivo* [16,17]. If Mn-MOF-74 particles accumulate in cancer sites through blood circulation, it may be used as an ideal metal ion pool to release Mn ions locally, thus promoting similar immunotherapy effect.

The degradation rate of MOF under physiological conditions is an important property to be considered in drug release performance of MOF [18, 19]. Ruyra et al. demonstrated that several nanoMOFs (such as UiO-67, ZIF-7, HKUST-1) become amorphous or decompose to release cations when exposed to cell culture medium [20]. Li et al. showed that the particle size of MIL-100 (FE) and MIL-101 (FE) determined the stability and biodegradability of MOF when exposed to phosphate buffer solution (PBS) [21]. The mechanism of MOF degradation is attributed to the affinity of phosphate group for multivalent cations, which is supported by the formation of new insoluble metal phosphates. In this study, nano-Mn-MOF-74 was synthesized by adding acetic acid to adjust the

crystal size, and the release rate of Mn ion was deduced by tracking the change of ligand concentration, so as to explore the degradation process of nano-Mn-MOF-74.

2. Materials and Methods

2.1. Preparation of nano-Mn-MOF-74

All reagents were purchased at Kemate Chemical Technology Co., Ltd. UV-vis spectra were recorded at a UV-Vis 2550 spectrophotometer (Shimadzu Corporation of Japan). Transmission Electron Microscopy were obtained in a FEI Talos F200X G2 microscope (FEI Czech company), and Scanning Electron Microscope were obtained in a JSM-7500F microscope (Hitachi, Japan). Phase analysis of xray diffraction were obtained in a Rigaku SmartLab analyzer (Rigaku Corporation).

2.2. Preparation of nano-Mn-MOF-74

2920 mg $MnCl_2 \cdot 4H_2O$ and 813.96 mg 2OH-BDO were dissolved in 352 mL DMF, then 23.4 ml CH_3CH_2OH, 23.4 mL ultra-pure water and 60 g CH_3COOH were added to the mixture, and the resulting mixture was put into an autoclave. Heat them in an oven at 135 °C for 24 hours. After the reaction, the product was collected and washed with DMF for three times. The product was immersed in CH_2Cl_2 for two days and replaced with fresh CH_2Cl_2 every day. Finally, the product was dried in the vacuum drying oven.

2.3. Degradation of nano-Mn-MOF-74

2.3.1. Determination of standard curve of 2OH-BDO

The standard solution of 2OH-BDO can be obtained by weighing 10 mg of 2OH-BDO by analytical balance and dissolving in 40 ml of ultra-pure water, then constant volume in 50mL volumetric flask and shaking well. 0.1 mL, 0.2mL, 0.4mL, 0.6mL, 0.8mL and 1 mL of the above standard solutions were taken respectively. The above-mentioned standard solutions were diluted to 5 mL by adding ultra-pure water respectively. After shaking, the 2OH-BDO solutions of 4 mg/L, 8 mg/L, 16 mg/L, 24 mg/L, 32 mg/L and 40 mg/L were obtained. After filtering one mL of the prepared solution through 220 nm filter membrane, the UV absorbance curve of the above solutions was measured under the same test conditions. The peak absorbance of 352 nm was taken, and the standard curve of 2OH-BDO was drawn with the concentration as the horizontal coordinate and absorbance as the vertical coordinate.

2.3.2. Preparation of phosphate buffer solution (PBS)

Dissolve 7.9 g NaCl, 1.02 g KC1, 0.24 g KH_2PO_4 and 1.44 g Na_2HPO_4 in 800 mL distilled water, adjust the pH value of the solution to 7.4 with HCl, finally add distilled water to 1 L, and store in 4 ℃ refrigerator.

2.3.3. Monitoring Mn release during degradation of nano-Mn-MOF-74 in PBS

10 mg nano-Mn-MOF-74 particles were ultrasonically dispersed in 50 mL PBS buffer, and the ultrasonic time should not be too long, just the sample was completely dispersed. After shaking at low speed, 5 mL solution was quickly taken out at specific time (0, 2, 4, 6, 8, 10, 12 h), centrifuged at 8000 rpm for 3 minutes, and the supernatant was taken out for ICP determination of Mn ion content.

2.3.4. Monitoring Mn release via dialysis acidification method during degradation of nano-Mn-MOF-74 in PBS

20 mg of nano-Mn-MOF-74 was dissolved in 5 mL ethanol by ultrasound. The mixture was placed in a dialysis bag (MWCO 10000) and then continuously stirred in 100 mL PBS buffer at 37 ℃. 4 mL of solution was sampled from the buffer outside the dialysis bag at a specific time (0, 2, 4, 6, 8, 10, 12 h) and mixed with 1 mL of 1 M nitric acid. The mixture was centrifuged at 8000 rpm for 3 minutes, and the content of Mn in the supernatant was analyzed by ICP.

2.3.5. Monitoring the release of 2 OH-BDO during the degradation of nano-Mn-MOF-74 in PBS

10 mg nano-Mn-MOF-74 particles were ultrasonically dispersed in 50 mL PBS buffer. After shaking at low speed, 5 mL solution was quickly taken out at a specific time (0, 2, 4, 6, 8, 10, 12 h), centrifuged at 8000 rpm for 3 minutes, and the supernatant was taken out to measure its absorbance with UV-vis spectrophotometer.

3. Experimental Results and Discussion

3.1. Preparation of nano-Mn-MOF-74

Nano-Mn-MOF-74 was prepared by introducing acetic acid as a regulator to adjust the size and crystal shape of MOF particles. According to the SEM and TEM images in the reported literature [22], the size of Mn-MOF-74 is generally in the micron level. As shown in Fig. 1, it can be seen that the nano-Mn-MOF-74 nanoparticles had a typical size of about 300 nm and polyhedral shape although most of them exist in the agglomerated state.
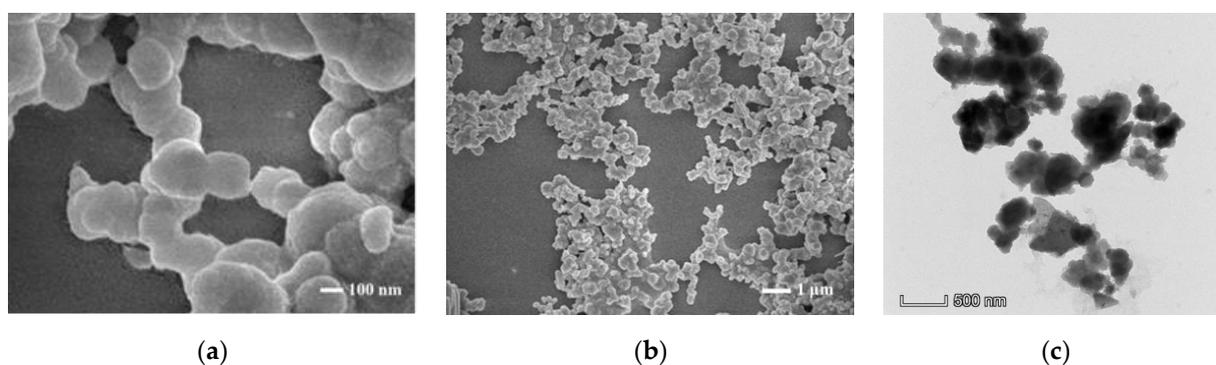

(**a**)   (**b**)   (**c**)

Figure 1. (**a**) and (**b**)SEM images of nano-Mn-MOF-74　（**c**）TEM image of nano-Mn-MOF-74

As shown in Figure 2, it can be seen that nano-Mn-MOF-74 prepared by us has high purity crystal structure. The Mn-MOF-74 has similar pattern with the simulated value [23], indicatesing that the size of the particles is mainly regulated by the modifier acetic acid. However, it has no effect on the crystal shape of the particles.
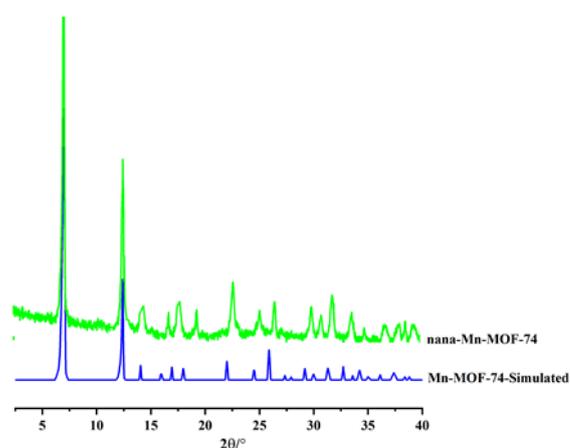

Figure 2. XRD patterns of nano-Mn-MOF-74

3.2. Degradation of nano-Mn-MOF-74

Based on the above characterization and analysis, nano-Mn-MOF-74 was taken as an example to explore the degradation process of nano-MOF under physiological conditions. As shown in Figure 3 of the ultraviolet visible absorption spectrum at different concentrations of 2OH-BDO. It can be confirmed that the ultraviolet absorption peak of 2OH-BDO is around 352 nm. According to the relationship between the peak value and the concentration, the standard curve of 2 OH-BDO is obtained as shown in Figure 4.
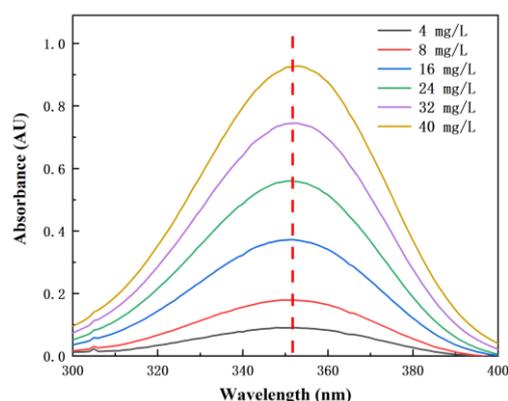

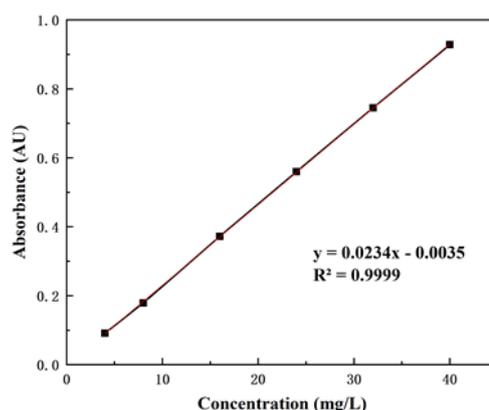**Figure 3.** Spectra of different concentrations of 2OH-BDO

Figure 4. Standard curve of 2OH-BDO

When nano-Mn-MOF-74 is degraded in PBS buffer, a large number of Mn ions will be released, and these Mn ions will precipitate with the phosphate in PBS buffer to form manganese phosphate [20]. Therefore, only a small amount of Mn ions can be detected in buffer, which will affect the calculation of degradation rate, showing extremely slow degradation rate. When dialyzing method is used, Mn ions released by nano-Mn-MOF-74 in dialysis bags will be precipitated with phosphate in PBS buffer outside the dialysis bag. Taking out PBS buffer mixture for acidizing will release Mn ions in precipitation again, and then will not affect the detection of degradation rate.
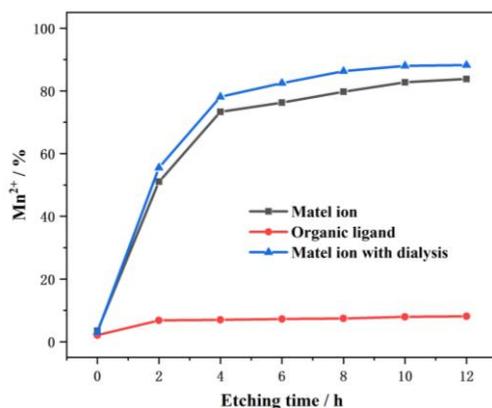
Figure 5. Degradation rate curve of nano-Mn-MOF-74

When the concentration of 2OH-BDO is detected, the problem of new precipitation can be avoided. After the absorbance of the solution is measured by UV-Vis spectrophotometer, the concentration of 2OH-BDO can be calculated according to the standard curve. According to the formula $[Mn_2(C_8H_2O_6)(H_2O_2)] \cdot 6.3H_2O$ of Mn-MOF-74 previously reported in the literature [24], the amount of Mn ions released in the degradation process of nano-Mn-MOF-74 can be calculated, and then the degradation rate can be calculated. As shown in Figure 5, the degradation rate obtained by the new method is basically the same as that obtained by dialysis acidification, which proves that the method of measuring the concentration of 2OH-BDO to calculate the degradation rate is feasible.

4. Conclusions

In conclusion, we used acetic acid as regulator to adjust the size and crystal shape of MOF particles, and then nano-Mn-MOF-74 was prepared. The metal ions and buffer solution will precipitate when the MOF is degraded under physiological conditions that will affect the calculation of degradation rate. The concentration of organic ligands in buffer solution was measured, and the metal ions released during MOF degradation according to the molecular formula of MOF and the degradation rate were calculated. This method developed here is feasible and effective, and it can be used in the study of degradation rate of other MOF under physiological conditions.

Institutional Review Board Statement: Not applicable.

Informed Consent Statement: Not applicable.

Data Availability Statement: No new data were created or analyzed in this study. Data sharing is not applicable to this article.

Conflicts of Interest: The authors declare no conflict of interest.

References

1. Yaghi, O., O'Keeffe, M., Ockwig, N. Reticular synthesis and the design of new materials. *Nature* 423, 705–714 (2003).
2. A. Carné, C. Carbonell, I. Imaz, D. Nanoscale metal–organic materials. *Chem. Soc. Rev.* 2011, 40, 291–305.
3. Trickett, C., Helal, A., Al-Maythalony, B. The chemistry of metal–organic frameworks for CO_2 capture, regeneration and conversion. *Nat Rev Mater* 2, 17045 (2017).

4. Diercks, C.S., Liu, Y., Cordova, K.E. The role of reticular chemistry in the design of CO_2 reduction catalysts. *Nature Mater* 17, 301–307 (2018).
5. C. He, D. Liu and W. Lin. Nanomedicine Applications of Hybrid Nanomaterials Built from Metal–Ligand Coordination Bonds: Nanoscale Metal–Organic Frameworks and Nanoscale Coordination Polymers. *Chem. Rev.* 2015, 115, 11079-11108.
6. Horcajada, T. Chalati, C. Serre, B. Gillet, C. Sebrie, T. Baati, J. F. Eubank, D. Heurtaux, P. Clayette and C. Kreuz. Porous metal–organic-framework nanoscale carriers as a potential platform for drug delivery and imaging. *Nat. Mater.* 2010, 9, 172-178.
7. S. Wang, C. M. McGuirk, A. d'Aquino, J. A. Mason and C. A. Mirkin. Metal–organic framework nanoparticles. *Adv. Mater.* 2018, 30, 1800202.
8. G. Lan, K. Ni, Z. Xu, S. S. Veroneau, Y. Song and W. Lin. Nanoscale metal–organic framework overcomes hypoxia for photodynamic therapy primed cancer immunotherapy. *J. Am. Chem. Soc.*, 2018, 140, 5670-5673.
9. X. Meng, J. Deng, F. Liu, T. Guo, M. Liu, P. Dai, A. Fan, Z. Wang and Y. Zhao. Triggered all-active metal organic framework: ferroptosis machinery contributes to the apoptotic photodynamic antitumor therapy. *Nano Lett.*, 2019, 19, 7866-7876.
10. K. M. Taylor, W. J. Rieter and W. Lin. Nanoscale coordination polymers for platinum-based anticancer drug deliver *J. Am. Chem. Soc.* 2008, 130, 14358-14359.
11. H. Jiang, C. Wang, H. Wang and M. Zhang. Synthesis of highly efficient MnOx catalyst for low-temperature NH_3-SCR prepared from Mn-MOF-74 template. *Mater. Lett.* 2016, 168, 17-19.
12. W. Zhou, H. Wu and T. Yildirim. Enhanced H_2 Adsorption in Isostructural Metal−Organic Frameworks with Open Metal Sites: Strong Dependence of the Binding Strength on Metal Ions. *J. Am. Chem. Soc.* 2008, 130, 15268-15269.
13. S. Zanganeh, G. Hutter, R. Spitler, O. Lenkov, M. Mahmoudi, A. Shaw, J. S. Pajarinen, H. Nejadnik, S. Goodman and M. Moseley. Iron oxide nanoparticles inhibit tumour growth by inducing pro-inflammatory macrophage polarization in tumour tissues. *Nat. Nanotechnol.* 2016, 11, 986-994.
14. L. S. Lin, J. Song, L. Song, K. Ke, Y. Liu, Z. Zhou, Z. Shen, J. Li, Z. Yang and W. Tang. Simultaneous Fenton-like Ion Delivery and Glutathione Depletion by MnO2-Based Nanoagent to Enhance Chemodynamic Therapy. *Angew. Chem.* 2018, 130, 4996-5000.
15. C. Liu, D. Wang, S. Zhang, Y. Cheng, F. Yang, Y. Xing, T. Xu, H. Dong and X. Zhang. Biodegradable Biomimic Copper/Manganese Silicate Nanospheres for Chemodynamic/Photodynamic Synergistic Therapy with Simultaneous Glutathione Depletion and Hypoxia Relief. *ACS Nano.* 2019, 13, 4267-4277.
16. Song, Y., Liu, Y., Teo, H.Y. Manganese enhances the antitumor function of $CD8^+$ T cells by inducing type I interferon production. *Cell Mol Immunol* (2020).
17. M. Lv, M. Chen, R. Zhang, W. Zhang, C. Wang, Y. Zhang, X. Wei, Y. Guan, J. Liu and K. Feng. Ameliorative effects of resveratrol against cadmium-induced nephrotoxicity via modulating nuclear xenobiotic receptor response and PINK1/Parkin-mediated Mitophagy. *Cell Res.* 2020, 1-14.
18. Li, X., Lachmanski, L., Safi, S. New insights into the degradation mechanism of metal-organic frameworks drug carriers. *Sci Rep* 7, 13142 (2017).
19. E. Bellido, M. Guillevic, T. Hidalgo, M. J. Santander-Ortega, C. Serre and P. Horcajada. Understanding the Colloidal Stability of the Mesoporous MIL-100(Fe) Nanoparticles in Physiological Media. *Langmuir.* 2014, 30, 5911–5920.
20. À. Ruyra, A. Yazdi, J. Espín, A. Carné-Sánchez, N. Roher, J. Lorenzo, I. Imaz and D. Maspoch. Synthesis, culture medium stability, and in vitro and in vivo zebrafish embryo toxicity of metal-organic framework nanoparticles. *Chem. – Eur. J.* 2015, 21, 2508–2518.
21. X. Li, L. Lachmanski, S. Safi, S. Sene, C. Serre, J. M. Grenèche, J. Zhang and R. Gref. New insights into the degradation mechanism of metal-organic frameworks drug carriers. *Sci. Rep.* 2017, 7, 13142.
22. H. Jiang, C. Wang, H. Wang and M. Zhang. Synthesis of highly efficient MnOx catalyst for low-temperature NH_3-SCR prepared from Mn-MOF-74 template. *Mater. Lett.* 2016, 168, 17-19.
23. Doufeng Wu, Wenqing Yan, Huoshu Xu, Erpan Zhang, Qiaowei Li. Defect engineering of Mn-based MOFs with rod-shaped building units by organic linker fragmentation. *Inorganica Chimica Acta.* 2017, 460, 93-98.
24. Wong-Ng, W., Kaduk, J., Wu, H., & Suchomel, M. (2012). Synchrotron X-ray studies of metal-organic framework M2(2,5-dihydroxyterephthalate), M = (Mn, Co, Ni, Zn) (MOF74). *Powder Diffraction,* 27(4), 256-262.